Selective observation of semi-rigid residues on the surface of dynamically complex mutant huntingtin protein fibrils

Irina Matlahov [a], Jennifer C. Boatz [b,1] and Patrick C. A. van der Wel [a,b,*]

[a] Zernike Institute for Advanced Materials, University of Groningen, Groningen, The Netherlands
[b] Department of Structural Biology, University of Pittsburgh School of Medicine, Pittsburgh, PA, USA

* Corresponding author: p.c.a.van.der.wel@rug.nl, phone +31 (0) 50 363 26 83; Nijenborgh 4, 9747AG Groningen, The Netherlands

[1] Present address: Division of Pulmonary and Critical Care Medicine, University of Pittsburgh School of Medicine, Pittsburgh, PA, USA

Highlights

- Mutant huntingtin exon 1 fibrils feature a broad range of molecular dynamics.
- Molecular motion is coupled to dynamics of the fiber-associated water solvent.
- Dynamics-based spectral editing ssNMR reveals mobile surface residues.
- Intermediate-motion selection uses dipolar-dephasing of rigid sites.
- Surface-facing glutamines outside the fiber core observed and identified.

Abstract

Many amyloid-forming proteins, which are normally intrinsically disordered, undergo a disorder-to-order transition to form fibrils with a rigid β-sheet core flanked by disordered domains. Solid-state NMR (ssNMR) and cryogenic electron microscopy (cryoEM) excel at resolving the rigid structures within amyloid cores but studying the disordered domains on fibril surfaces remains more challenging. This challenge is exemplified by a fragment of mutant huntingtin exon 1 (HttEx1), which self-assembles into pathogenic neuronal inclusions in Huntington disease (HD). The mutant protein's expanded polyglutamine (polyQ) segment forms a highly rigid fibril core with dynamic surface residues and disordered 'flanking' segments. Here we deploy dynamically sensitive magic angle spinning ssNMR experiments and variable temperature studies to elucidate how solvent dynamics impact the fibrils' segmental dynamics, and permit the identification of surface-facing (polyQ) residues. A novel implementation of dynamic spectral editing (DYSE) ssNMR is described and applied, in order to reveal the weak signals of surface-facing glutamine residues despite the strong background of rigid core signals. This type of 'intermediate motion selection' (IMS) experiment, based on cross-polarization (CP) ssNMR, is complementary to more traditional DYSE methods that highlight highly flexible or highly rigid protein segments. Integration of the IMS-DYSE element in standard CP-based ssNMR experiments permits the observation of previously invisible fiber surface signals and may be extended to a wider variety of biomolecular assemblies and (bio)materials. In pathogenic protein amyloid fibrils the detection of surfaces of the (polyQ) amyloid core is relevant to e.g. the development of fluorescent dyes and positron emission tomography tracers that selectively bind these surfaces.

Keywords: intermediate-timescale motion; solid state NMR; Huntington's disease; polyglutamine

Abbreviations:

AD, Alzheimer's disease, CP, cross polarization, cryo EM: cryogenic electron microscopy, DARR: dipolar assisted rotational resonance, DCP: double CP, DIPSHIFT: dipolar chemical shift, DYSE: dynamic spectral editing, HD: Huntington's disease, HttEx1: huntingtin exon 1, httNT: N-terminal domain of htt, IMS-DYSE: intermediate-motion selection dynamic spectral editing, INEPT: insensitive nuclei enhanced by polarization transfer, MAS: magic angle spinning, MBP: maltose-binding protein, MBP-Q44-HttEx1: maltose-binding protein bound to huntingtin exon 1 which includes 44 glutamines in its polyglutamine domain, PD: Parkinson's disease, PDSD: proton-driven spin diffusion, PET: positron emission tomography, polyQ: polyglutamine, PPII: polyproline II, PRD: proline-rich domain, Prc: prolines in random coil conformation, REDOR: rotational echo double resonance, ssNMR: solid-state nuclear magnetic resonance, T_2: transverse relaxation, TEDOR: transferred echo double resonance, TPPM: two-pulse phase modulated proton decoupling.

Introduction

Self-assembled protein filaments play major roles in nature, with amyloids or amyloid-like structures now known to arise in many places in the human body. Sometimes amyloid-like fibrils are products of evolution, enabling specific biological functions involving either reversible or irreversible assemblies (Fowler et al., 2007; Muiznieks et al., 2018). More famous are the pathogenic amyloids that are culprits of neurodegenerative aggregation diseases like Alzheimer's disease (AD), Parkinson's disease (PD), and Huntington's disease (HD) (Chiti & Dobson, 2017). Recent decades have seen dramatic developments in the structural studies of these types of fibrillar assemblies, with breakthrough structures resolved by first solid-state NMR spectroscopy (ssNMR) and more recently cryogenic electron microscopy (cryoEM) (Fitzpatrick et al., 2017; Fitzpatrick & Saibil, 2019; Hervas et al., 2020; Lutter et al., 2021; van der Wel, 2017a). This has revealed that these fibrils feature a variety of β-sheet based fibril cores, which are internally remarkably well ordered, even when a single protein can often form distinct fibril strains (or polymorphs).

Within polymorphic fiber architectures, the focus is typically on differences in the structure of the cross-β fiber core. However, segments or domains outside this core region play a critical role in the misfolding process and are necessary for determining the functional (and toxic) properties of the resulting aggregates. These 'flanking' regions do not partake in the β-sheet fiber core, and therefore are typically surface exposed and mediate interactions with other cellular components (Lin et al., 2017; Ulamec et al., 2020). As such, flanking domain accessibility and interactions can be crucial for identifying toxic fibril polymorphs. Moreover, such domains represent targets or 'epitopes' for chaperones to bind, thereby controlling the stability and turnover of misfolded protein deposits (Wentink et al., 2020). Besides the disordered flanking segments, the surfaces of the fiber core itself are of interest. In a diagnostic context, the fiber surfaces are important targets for amyloid-specific fluorescent dyes and tracers used in positron emission tomography (PET) (Fändrich et al., 2018). Thus, a detailed understanding of structural features on the fibril surface is of substantial biomedical interest.

Resolving the non-core parts of amyloid fibrils is a substantial challenge. Unlike the amyloid core itself, the surface features are usually dynamically and statically disordered. Consequently, flanking domains are often effectively invisible in cryoEM density maps, and if they do show up they cannot be fully resolved. Fortunately, ssNMR offers various techniques that can detect and characterize these surface features. Most notably, one can borrow approaches from solution NMR to study in great detail highly flexible and disordered regions within flanking domains (Falk et al., 2020; Helmus et al., 2010; Matlahov & Wel, 2018). However, this approach is limited to segments with very high flexibility, and it fails for (folded) protein regions that partly immobilized on the fiber surface. Such structural elements display intermediate mobility, in-between the rigid core and flexible tails, rendering them difficult to detect by the most commonly used ssNMR techniques (more below). Yet, segments of intermediate mobility can have important biological roles. For instance, pathogenic and functional amyloids can be decorated with (partially) folded domains that have important functional properties, e.g. by acting as binding partner

recognition sites or by having enzymatic activity. Moreover, structured motifs on the fibril surface can be targeted for polymorph-specific diagnostics or targeted protein degradation efforts (Fändrich et al., 2018; Tao et al., 2022).

The pathogenic protein aggregates formed by mutant huntingtin (Htt) fragments implicated in HD could similarily be targeted by their intermediate mobility surface features (Bates et al., 2015). In this inherited neurodegenerative disease, the N-terminal fragments of mutant Htt form ordered protein aggregates, which are found as cytoplasmic and nuclear inclusions in patient neurons (Macdonald, 1993). Recent cryoEM studies have revealed the native fold of Htt, yielding a structure that lacks information on up to 25% of the sequence (Bäuerlein et al., 2017; Guo et al., 2018; Matlahov & Wel, 2019). These "invisible" flexible regions include the first exon 1 (HttEx1) which bears the HD mutation site.

The mutant HttEx1 fragment is detected in patients and is highly aggregation prone. In model animals, in cultured cells, and *in vitro*, mutant HttEx1 undergoes a pathogenic disorder-to-order transition that is connected to the HD mutation: expansion of the polyglutamine (polyQ) domain (Scherzinger et al., 1997). Notably, HD is but one of a whole family of polyQ expansion or CAG repeat expansion disorders (Bates et al., 2015). The structure of polyQ-expanded HttEx1 aggregates has been studied by many techniques (Bäuerlein et al., 2017; Bugg et al., 2012; Caulkins et al., 2018; Duim et al., 2014; Galaz-Montoya et al., 2021; Guo et al., 2018; Hoop et al., 2014; Isas et al., 2019; Sivanandam et al., 2011). However, the HttEx1 fibrils have not permitted an atomic level structure to be determined, due at least in part to inherent disorder within the fiber core and the flexible domains decordating its surface (Figure 1A). Internally, the polyQ core domain is ordered, rigid and sequestered from solvent molecules (Hoop et al., 2016; Matlahov & Wel, 2019; Schneider et al., 2011). Residues outside the central core display higher mobility and solvent exposure, which are most notable for the flanking segments on either side of the polyQ: the N-terminal (htt^{NT}) and C-terminal proline rich domains (PRD) (Bugg et al., 2012; Lin et al., 2017) (Figure 1A). In some fibrils, the htt^{NT} adopts a dynamic α-helical structure (shown as dark blue cylinders), while in other proteins it is in a disordered and flexible state (Boatz et al., 2020; Isas et al., 2015). The PRD domain contains two PPII helical structures (light blue cylinders) along with a C-terminal tail, with the former partly mobile but the latter highly flexible (Bugg et al., 2012; Caulkins et al., 2018; Lin et al., 2017). Thus, there is a remarkable gradient of mobility, from the rigid fiber core to the extremely dynamic C-terminal tail. Moreover, the dynamics of the flanking domains vary depending on the supramolecular polymorphism of the fibers, with implications for the fibrils' toxic properties (Khoshnan et al., 2002; Legleiter et al., 2009; Lin et al., 2017; Southwell et al., 2008).

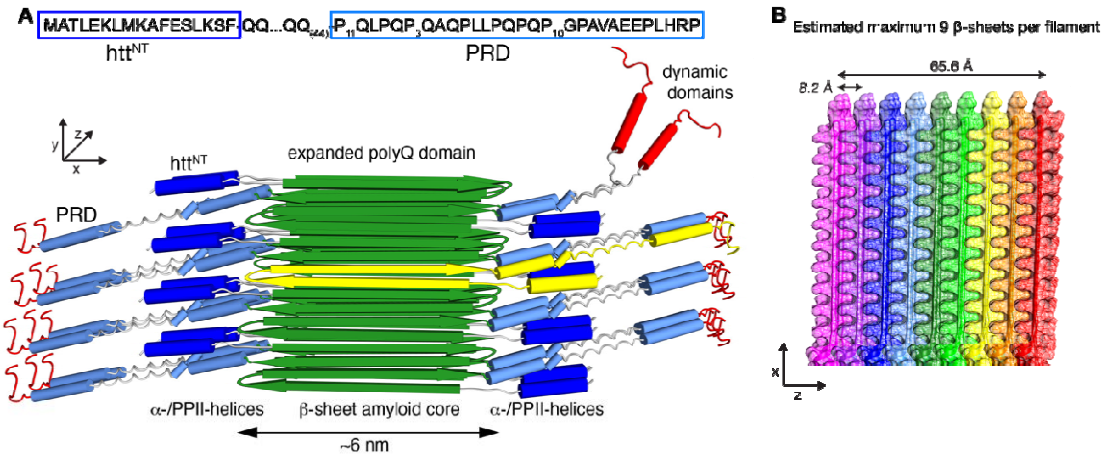

Figure 1. Fibril architecture of aggregated mutant HttEx1. (A) Structural model of HttEx1 fibers. The xyz scale demonstrates the fiber growth direction (y), fiber width (x) and the depth of the fiber (z). (B) Structural model of HttEx1 fibers showing interdigitation of the Gln core. According to transmission electron micrographs, the fiber depth (z direction) is approximately the same as the β-strand length and composed of several stacked β-sheets. Each β-sheet is shown in different colour demonstrating that the 6-7 nm filament core is composed of around nine stacked β-sheets. Figure adapted with permission from ref. (Lin et al., 2017) and (Boatz et al., 2020), under the Creative Commons CC-BY license.

Our current understanding of the fibril structure stems from an integration of structural biology techniques, with a prominent role for ssNMR spectroscopy. Of particular importance have been ssNMR experiments that distinguish the rigid core from the flexible surface, enabled by dynamic spectral editing (DYSE) techniques (Matlahov & Wel, 2018). With some exceptions (Kashefi et al., 2019), the DYSE methods usually are focused on reveling either highly mobile residues or the most rigid parts of the sample. DYSE techniques, in both 1D and 2D spectroscopy, have proved effective for many different protein assemblies (Helmus et al., 2008; Murray et al., 2017; van der Wel, 2017b, 2018). On the one hand, INEPT-based ssNMR excels at revealing highly flexible (mostly random coil) flanking domain segments, which have long transverse relaxation times (T_2). Conversely, the rigidity of the fiber core allows it to be studied in cross-polarization (CP) based ssNMR. CP ssNMR utilizes the dipolar couplings between nuclei, which requires a lack of (fast) isotropic motion that otherwise negates the dipolar interactions.

Yet, it has remained challenging to observe and study residues or segments with an intermediate mobility. Some partly immobilized domains (that are not fully rigid) can be detected by CP-based ssNMR (Helmus et al., 2010; Ryder et al., 2021), although at reduced intensity. The signals from such semi-mobile domains are often masked by stronger signals from more rigid parts of the protein structure. In HttEx1 fibrils studied by CP ssNMR, most of the polyQ ssNMR signal reflects the rigid dehydrated core with crystal-like rigidity. Yet, there is also a direct polyQ-core-solvent interface (Figure 1B) that is of real interest, as it harbors binding sites for amyloid-specific dyes (like congo red or thioflavin T) and PET ligands designed for *in vivo* imaging of mutant Htt (Bertoglio et al., 2021; Liu et al., 2020). Moreover, the fiber core surface may be implicated in secondary nucleation events that play a prominent role in aggregation of HttEx1 and other amyloidogenic polypeptides (Boatz et al., 2020; Wagner et al., 2018).

In this work, we set out to gain more insight into the functionally relevant, but difficult-to-observe segments and residues on the HttEx1 fiber surface. We deploy variable temperature ssNMR studies to probe the role of solvent dynamics in modulating the mobility of the fibrils, juxtaposing the fiber core and surface domains. Moreover, we deploy a new DYSE method that combines two previously reported techniques (^{1}H-^{13}C DIPolar chemical SHIFT (DIPSHIFT) and ^{13}C-^{13}C Dipolar Assisted Rotational Resonance (DARR) experiments (Munowitz et al., 1981; Takegoshi et al., 2001)), to selectively probe the semi-mobile residues on the fiber surface. This approach aims to reduce the disadvantageous dynamic noise problem affecting the detection of semi-mobile surface glutamines by partly or fully suppressing the signals from rigid polyQ core residues, complementing a recently reported technique based on other types of dipolar interactions (Kashefi et al., 2019). With this technique we can identify otherwise invisible signals of glutamine residues on the fiber core surface, distinct from the dominant rigid core that normally dominates the CP-based ssNMR spectra.

Materials and Methods

Protein expression, purification, and fibrillation

Mutant huntingtin exon 1 with a 44-residue polyQ core was expressed as part of a maltose binding protein (MBP) fusion protein as previously reported (Hoop et al., 2014; Lin et al., 2017). The fusion protein MBP-Q44-HttEx1 was subcloned into a pMalc2x plasmid by Genscript. The protein expression was done in *Escherichia coli* BL21(DE3) pLysS cells (Invitrogen, Grand Island, NY). Samples for MAS ssNMR were uniformly ^{13}C, ^{15}N labeled with ^{13}C D-glucose and ^{15}N ammonium chloride. After protein expression, cells were pelleted at 7000g, resuspended in phosphate buffered saline (PBS) (SKU BP399-4, Fisher BioReagents, Pittsburgh, PA) and lysed in presence of 1 mM phenylmethanesulfonyl fluoride (PMSF) (SKU 215740050, Acros Organics, New Jersey, USA) by an M-110Y high pressure pneumatic high shear fluid processor (Microfluidics, Newton, MA). Subsequently, cells were centrifuged at 38,720g for 1h using a Sorvall RC 3C Plus centrifuge (Thermo Scientific, Waltham, MA). The supernatant that contained the soluble fusion protein was filtered over Millex-GP syringe-driven 0.22-μm PES membranes (Millipore Sigma, Burlington, MD). The fusion protein was purified by fast protein liquid chromatography (FPLC) using a 5ml HisTrap HP nickel column (GE Healthcare, Uppsala, Sweden) with 0.5M imidazole gradient (SKU I5513-100G, Sigma, St. Louis, MO) on an AKTA system (GE Healthcare, Chicago, IL). The imidazole was removed from the purified protein using an Amicon Ultra centrifugal filter with a regenerated cellulose membrane (Millipore Sigma, Burlington, MA). At least 3 washes with imidazole-free PBS buffer were done. Protein concentration was calculated from the absorbance at 280nm. According to ProtParam tool by ExPasy (Gasteiger, 2003) the extinction coefficient of the fusion protein is 66,350 $M^{-1}cm^{-1}$. Factor Xa protease (SKU PR-V5581, Promega, Madison, WI) was used to cleave MBP-Q44-HttEx1 at 22 °C (Lin et al., 2017) to release Q44-HttEx1. After 3 days the obtained fibrils were washed with PBS to remove the cleaved MBP.

NMR experiments

The hydrated U-^{13}C,^{15}N-labeled Q44-HttEx1 fibrils were packed into a 3.2mm ssNMR rotor (Bruker Biospin) by sedimentation, using a previously described ultracentrifugal packing tool (Mandal et al., 2017). Experiments were performed on a wide-bore Bruker Avance-I 600 MHz spectrometer at 277K, 270K, 263K and 256K temperatures using a triple-channel (HCN) 3.2mm MAS EFree probe. All ^{13}C-detected experiments were done using two-pulse phase modulated (TPPM) proton decoupling of 83 kHz during acquisition (Bennett et al., 1995). Direct excitation ^{1}H MAS NMR experiments were performed using a 3μs 90° pulse on ^{1}H and recycle delay of 2.8s. 1D ^{13}C direct excitation experiments were done using a 90° ^{13}C pulse of 4μs and a 3s recycle delay, along with high power ^{1}H decoupling during acquisition. 1D ^{13}C cross-polarization (CP) experiments were done using a 3μs 90° pulse on ^{1}H, a contact time of 1ms, recycle delay of 3s. 2D ^{13}C-^{13}C DARR experiments (Takegoshi et al., 2001) were performed using a 3μs 90° pulse on ^{1}H, 4 μs 90° pulses on ^{13}C, a ^{1}H-^{13}C CP contact time of 1ms or 750 μs at 277 and 256K respectively, a DARR mixing time of 25ms, and a recycle delay of 2.8s. A 2D PDSD (proton-driven spin diffusion) experiment was done at 256K using same pulses as in 2D DARR experiment but with a mixing time of 500ms. 2D ^{13}C-^{15}N NCO experiments were done using a 3μs 90° pulse on ^{1}H, 8μs 180° pulse on ^{13}C, ^{1}H-^{15}N contact time of 1.5ms (277K) and 800μs (256K), ^{15}N-^{13}C contact time of 4ms and recycle delay of 2.8s. 2D ^{13}C-^{15}N NCA experiments were done using a recycle delay of 2.8s, 3μs 90° pulse on ^{1}H, 8μs 180° pulse on ^{13}C, 1.5ms (277K) and 800μs (256K) and 4ms ^{1}H-^{15}N and ^{15}N-^{13}C contact times, respectively. The 1D DIPSHIFT experiments (Munowitz et al., 1981) were performed according to previously reported procedures (Hoop et al., 2014; Lin et al., 2017). This involved the use of a $R18_1^7$ R-sequence (Zhao et al., 2001) for ^{1}H-^{13}C dipolar protein recoupling. The 2D DIPSHIFT-DARR experiments were performed using recycle delay of 2.8s, 3μs 90° pulse on ^{1}H, 4 and 8μs 90° and 180° ^{13}C pulses respectively, 750μs ^{1}H-^{13}C contact time, 25ms mixing time. The ssNMR measurements were performed using Bruker Topspin software. Spectral processing and analysis were done using Topspin, CcpNMR Analysis (Skinner et al., 2016), as well as MestreNova software. Peak integration and peak deconvolution in the 1D slices were done using MestReNova. The chemical shifts were referenced relative to aqueous DSS using indirect referencing to the ^{13}C signals of adamantane (Harris et al., 2008; Morcombe & Zilm, 2003). Additional experimental details are tabulated in the Table S4 in the supporting information.

Results

Variable dynamics of distinct segments in the fibrils

We have previously described our protocols for generating amyloid-like fibrils from the mutant HttEx1 protein outfitted with a 44-residue polyQ segment (Q44-HttEx1), a common expansion length in HD patients (Hoop et al., 2014; Lin et al., 2017). Semi-rigid parts of the polyQ segment, as well as N- and C-terminal flanking domains, cover the fiber surface, but remain incompletely understood. First, we describe our use of variable temperature ssNMR studies to probe how solvent motion impacts the rigid and

semi-rigid fiber components, using ^{13}C,^{15}N-labeled Q44-HttEx1 fibrils. These ssNMR samples contain fully hydrated protein fibrils, with an excess of buffer that permits free motion of the surface exposed amino acid segments. **Figure 2** (top) shows the 1D ^{13}C spectra at 277K, obtained with either CP-based ssNMR (**Figure 2**A) or direct excitation (**Figure 2**B), which are differently sensitive to mobility. Rigid sites dominate the CP spectra, with high flexible residues being invisible. The direct excitation ssNMR shows rigid and mobile sites alike. Based on prior 2D ssNMR we can attribute assignments to the peaks (marked in **Figure 2**). The most rigid sites (high peaks in **Figure 2**A) are from the polyQ core (composed of two Gln conformers marked Qa and Qb), while increased mobility is seen for the htt^{NT} and PRD (which are higher in the direct excitation spectrum).

Upon freezing of the surrounding water, we expected dynamics of the protein to reduce, with a pronounced impact on especially solvent-interacting surface-exposed residues (Mandal et al., 2015; Mandal & van der Wel, 2016). Water reach freezing between 270 and 263K (as shown below). We observe an increase in the CP signal for the surface-facing protein segments (Htt^{NT} and PRD), which normally show reduced intensities due to dynamic averaging of the dipolar interaction (Figure 2A; 256K). Signal intensity increased in the methyl group region (10-25 ppm) and for the proline signals (marked with "P"). The signals were also broadened at low temperature, reflecting a freezing out of heterogeneous conformations. Peaks from the polyQ domain also increased in intensity upon freezing (Figure S1 A). This was surprising, since the fiber core is known to be devoid of water and is highly rigid (Schneider et al., 2011; Sivanandam et al., 2011). The observed additional rigidification upon freezing of the water phase may stem from semi-rigid glutamine residues on the polyQ core surface, as we discuss further below.

The ssNMR signals from the fiber core show equal amounts of two types of glutamine ("Qa" and "Qb"; **Figure 2**A), reflecting two differently structured β-strands in the Q44 β-hairpin (Hoop et al., 2016). Deconvoluted signals of the aliphatic glutamine carbons are shown in Figure S2 A-D, and signal widths and peak areas are indicated in Table S1. The line width of the Qa signal was unaffected, and the Qb signal showed only small changes in width. This shows that these glutamine signals reflect residues with high degree of inherent order, with no evidence of a freezing out of disordered conformations (Table S1). The fact that we observe a small change in linewidth of the Qb backbone and a slightly increased intensity, indicates an initially higher degree of motion of the Qb residues compared to Qa (or a stronger coupling to the solvent).

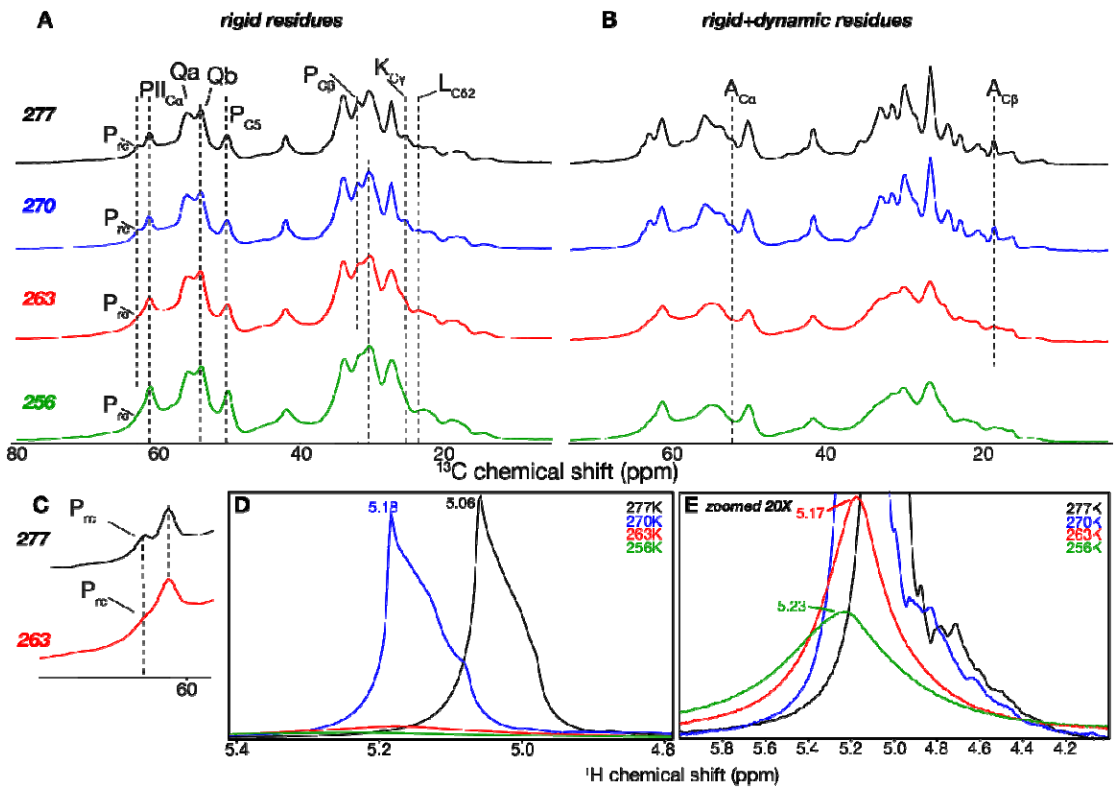

Figure 2. Variable temperature 1D MAS ssNMR of Q44-HttEx1 fibrils. (A) 1D ^{13}C CP-MAS ssNMR at 277, 270, 263 and 256K, reflecting signals of rigid or immobilized parts of the fibrils. (B) 1D ^{13}C direct excitation MAS ssNMR showing signals of both rigid and mobile residues. All data acquired at 600 MHz (^{1}H) and 10kHz MAS rates. Assignments are based on (Lin et al., 2017). (C) Comparison of Cα signal for random coil (rc) and PPII prolines. (D) ^{1}H NMR of water molecules at 277K (black), 270K (blue), 263K (red), 256K (green), as indicated. (E) Same data as panel D, zoomed 20X to show low intensity signals at 263 and 256K.

The Pro signals from the PRD underwent pronounced changes upon sample cooling. An increase in the CP signal (Figure S1 A) indicates reduced mobility at low temperatures. When discussing these changes, it is important to note the presence of signal from both polyproline II (PII) and random coil prolines (Prc). As previously discussed (Lin et al., 2017), these two Pro populations are most easily distinguished by the Cα signals (marked $PII_{C\alpha}$ vs Prc in Figure 2A) just above 60 ppm. A high cooling-induced increase in intensity was observed for the $PII_{C\alpha}$ peak, whilst at 263K the signal of the random coil prolines, Prc, was not resolved any further (**Figure 2**C). This is consistent with the latter reflecting flexible residues (Caulkins et al., 2018; Lin et al., 2017) becoming trapped in a broad range of conformations and leading to extreme signal broadening (estimated as peak width doubling to 480 Hz; Figure S2, Table S1). In contrast, only modest increases affected the line width of $PII_{C\alpha}$ (210 to 240 Hz) and $PII_{C\delta}$ signal from 0.19 to 0.24 kHz (Figure S2; Table S1). These findings provide additional support to the distinct levels of order in the different parts of the PRD (Bugg et al., 2012; Caulkins et al., 2018; Falk et al., 2020; Lin et al., 2017).

Solvent interactions and dynamics

To directly assess the connection between the changes in protein motion and solvent dynamics, we used ^{1}H-detected MAS ssNMR to monitor the solvent mobility as a function of temperature (Böckmann et al., 2009; El Hariri El Nokab et al., 2022; Mandal & van der Wel, 2016). **Figure 2**D shows the 1D proton spectra of the same fibril sample between 277 and 256K. At 277 and 270K the ^{1}H signal was strong, indicating rapid motion for the majority of detected water molecules. Signal deconvolution suggested co-existence of four peaks (Figure S3), reminiscent of the multiple water pools reflecting bulk water, peptide-bound water and interfibrillar water (Table S2) detected in Aβ40 fibril samples (Wang et al., 2017). The narrowest signal corresponded to bulk water (Figure S3 A, signal number 1) with a longer T_2 relaxation time (narrower peak) at 277K compared to 270K (Figure S3 B, signal number 1). The signal shifts from 5.06 to 5.18ppm (between 277 and 270K), consistent with the known temperature dependence of the water chemical shift (Schmidt et al., 2006). At 263K the signal intensity drastically lowered by ~70% compared to the 277K signal (**Figure 2**D red) indicating a phase transition of bulk water from liquid to solid. A residual water signal at 5.17 ppm (**Figure 2**E) was from a subpopulation of water molecules that resist freezing, but did have a broadened peak width and very short T_2 relaxation times (Table S2), demonstrating constrained mobility. These are expected to be water molecules close to the protein (Böckmann et al., 2009). At 256K the water signal weakened by ~75% compared to the original intensity at 277K and broadened further, indicating a progressive immobilization of the water molecules close to fibrils. Overall, these results demonstrate the different dynamics of solvent molecules around the HttEx1 fibrils, as detected by the water phase transitions, and support the idea that the changes in protein motion (seen by ^{13}C NMR) are coupled to the water motional changes.

2D ssNMR of local fibril order and disorder

Next, a more detailed analysis of the temperature-related changes in the protein was obtained from 2D ssNMR experiments at 277 and 256K, above and below the solvent freezing temperatures (**Figure 3**A, B). The two spectra have many features in common. The dominant ssNMR signals of both a- and b-type glutamines were easily recognized at both 277 and at 256K (Cα-Cβ cross-peaks marked red ('a'-type) and blue ('b' type)). The line widths of these polyQ-core signals Qa and Qb showed only negligible changes between high and low temperature (Table 1). This finding is consistent with their participation in the fiber core, with limited contact with the (freezing) solvent. At 277K a much weaker signal from a third type of glutamines (Qc in Figure) was observable, previously attributed to non-core glutamines (Hoop et al., 2016; Isas et al., 2015, 2017; Sivanandam et al., 2011). Notably, at 256K, this signal disappeared, suggesting it broadened upon water freezing, providing support for the idea that it must stem from residues residing on the fiber surface (Helmus et al., 2008).

The Htt^{NT} and PRD, N- and C-terminal segments of HttEx1 are exposed outside the fiber core. The PRD segment's proline signals display a notable peak broadening in the 2D spectra, with different effects on the PPII helix and random coil prolines (PII, Prc). The cross peaks become stronger with temperature reduction, reflecting a more efficient polarization transfer as the motion-induced dipolar averaging was removed. The

signals also clearly increased in linewidth, with effects quantified by analyzing 1D slices extracted for the $^{13}C\alpha$ frequency of the random coil and PPII prolines, separately (**Figure 3**C-D;

Table 2). Interestingly, the line broadening differed somewhat among the different carbons, with the smallest changes seen for the Cδ linewidth in PPII (**Figure 3Error! Reference source not found.**C top,

Table 2). Unlike the PPII signals, the Pro in the random coil conformation (**Figure 3**D bottom) showed weaker cross-peaks (especially for the long-range transfer to Cδ), and more pronounced heterogeneity (e.g. two carbonyl signals; **Figure 3**C). At 256K there are no changes in line widths of the Prc signals except for Cβ (Table 3). The effect is even better seen in long range magnetization transfer at 256K where Prc signals totally disappeared, but PII became stronger (Figure S4). Additional backbone and side chain correlations were observed between prolines in the PPII helix conformation and both glutamine types. Thus, the PPII and Prc prolines experience distinct mobilities, with the random coil signals showing continued evidence of dynamics even at the lowest measurement temperature. This may relate to continued dynamics in hydration waters that resist freezing even at this temperature (see below).

A variety of peaks from the Htt^{NT} segment were observed in the 2D spectrum measured at 277K. This includes well-resolved signals from various methyl-bearing aliphatic amino acids, as well as Lys (see ref. (Lin et al., 2017)). Whilst we saw an increase in a few peaks from Ala Cα-Cβ (near 20 x 55 ppm) upon sample freezing, many of the other cross-peaks (near the diagonal between ca. 38 to 22 ppm) became less apparent due to excessive broadening. These observations contrasted with the signals of the more ordered polyQ and even PPII proline residues, and therefore reinforce the idea that the Htt^{NT} segment has a partly unstable secondary (α-helical) structure characterized by a high degree of mobility.

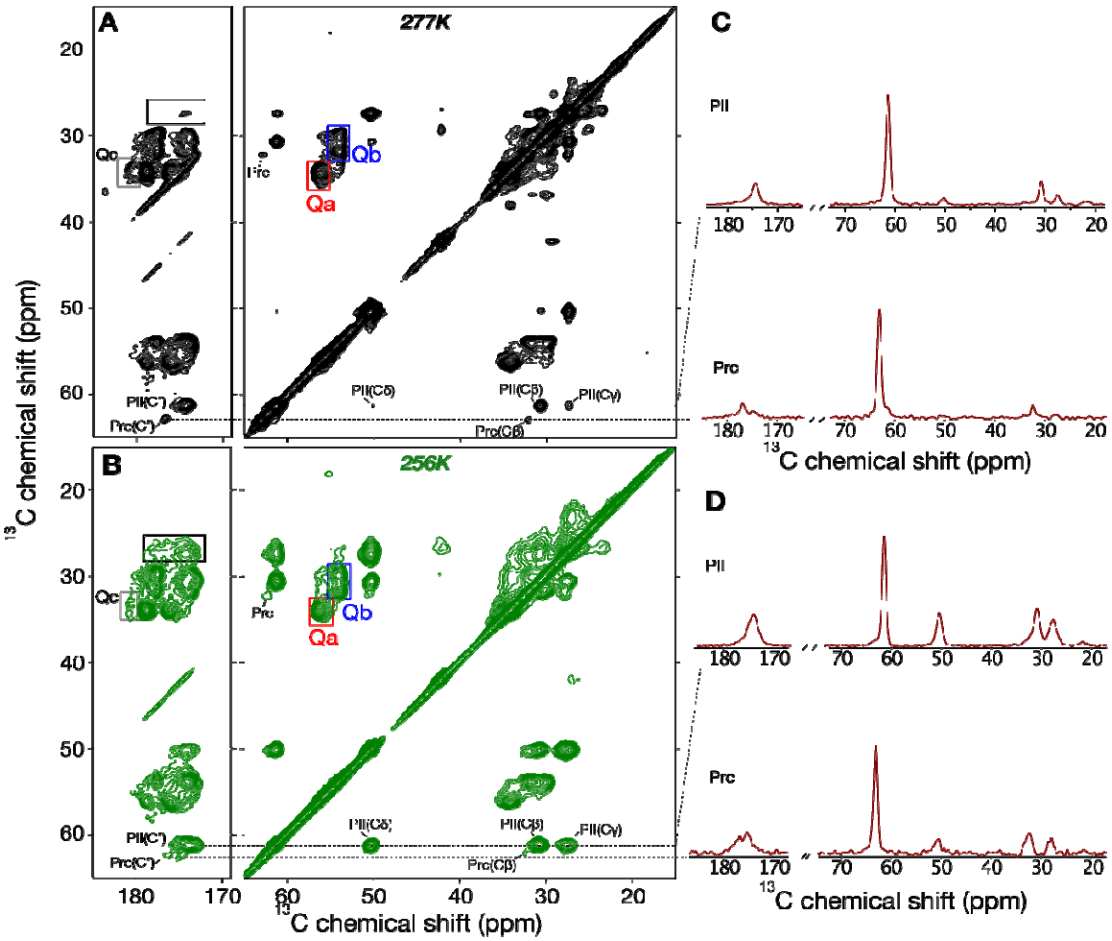

Figure 3. 2D ^{13}C-^{13}C DARR of Q44-HttEx1 fibrils. (A) 277K and (B) 256K. (C) 1D slices of proline signals located at PPII helix conformation (PII) and in the random coil conformation (Prc) at 277K. (D) 1D slices of proline signals located at PPII helix conformation (PII) and in the random coil conformation (Prc) at 256K.

Table 1. Linewidths extracted from 2D experiment for two glutamine types.

Residues	Qa line widths (kHz)		Qb line widths (kHz)	
	277K	256K	277K	256K
Cα	0.12	0.10	0.12	0.10
Cβ	0.17	0.18	0.18	0.19
Cγ	-	-	0.18	0.19
Cδ	0.16	0.18	0.13	0.14
C′	0.18	0.23	0.18	0.19

Table 2. Peak widths, chemical shifts and peak volume changes for prolines in PPII helixes in the PRD domain. *The values were derived by fitting 1D slices corresponding to the Cα frequency from **Figure 3**C.

	277K			256K		
	Chemical shifts (ppm)	Line widths (kHz)	Peak volume	Chemical shifts (ppm)	Line widths (kHz)	Peak volume
Cα*	61.42	0.15	2.4e9	61.43	0.14	1.2e9
Cδ	50.36	0.18	1.4e8	50.42	0.20	4.9e8
Cβ	30.85	0.14	6.1e8	30.94	0.21	8.0e8
Cγ	27.56	0.16	1.8e8	27.67	0.26	4.1e8
C′	174.50	0.23	9.4e8	174.18	0.37	9.3e8

Table 3. Peak widths, chemical shifts and peak volume changes for prolines in random coil conformations (Prc) in the PRD domain. *The values were derived by fitting 1D slices at the Cα frequency from **Figure 3**D.

	277K			256K		
	Chemical shifts (ppm)	Line widths (kHz)	Peak volume	Chemical shifts (ppm)	Line widths (kHz)	Peak volume
Cα*	63.08	0.14	1.7e9	63.06	0.14	4.8e8
Cδ	-	-	-	50.70	0.22	1.1e8
Cβ	32.39	0.13	2.1e8	32.54	0.24	1.2e8
Cγ	-	-	-	28.10	0.20	7.3e7
C′1	176.89	0.21	3.6e8	176.80	0.22	1.4e8
C′2	174.61	0.24	9.3e7	175.20	0.24	1.1e8

Variable temperature 2D ^{15}N-^{13}C spectra

2D double cross-polarization (DCP) experiments based on ^{1}H-^{15}N and ^{15}N-^{13}C CP steps were performed at 277 and 256K. At ambient temperatures, increased backbone mobility impacts both CP steps leading to losses of signal intensity for dynamic residues (Helmus et al., 2008). **Figure 4**A,B compares the 2D NCO and NCA spectra at 277 and 256K. At 277K, the spectra are dominated by signals from the polyQ amyloid core, with no strong signals from the flanking domains. The lack of signal for the latter stems from a combination of solvent-coupled dynamics and the lack of N-H protons in the prolines. The impact of low temperatures on these spectra are more striking than in the ^{13}C-^{13}C 2D spectra. At low temperature many additional signals were detected that were not seen at 277K, showing the improved polarization transfer in absence of molecular motion (**Figure 4**B marked with arrows). Many of these signals are very broad, including for instance an observed glycine signal. The prolines themselves become visible due to improved long-range polarization transfer overcoming the lack of direct protonation of the backbone nitrogen. In line with observations in other spectra above, both sidechain and backbone proline signals had widths of 0.17 and 0.19 kHz, indicating a well-ordered PPII helical structure (**Figure 4**B).

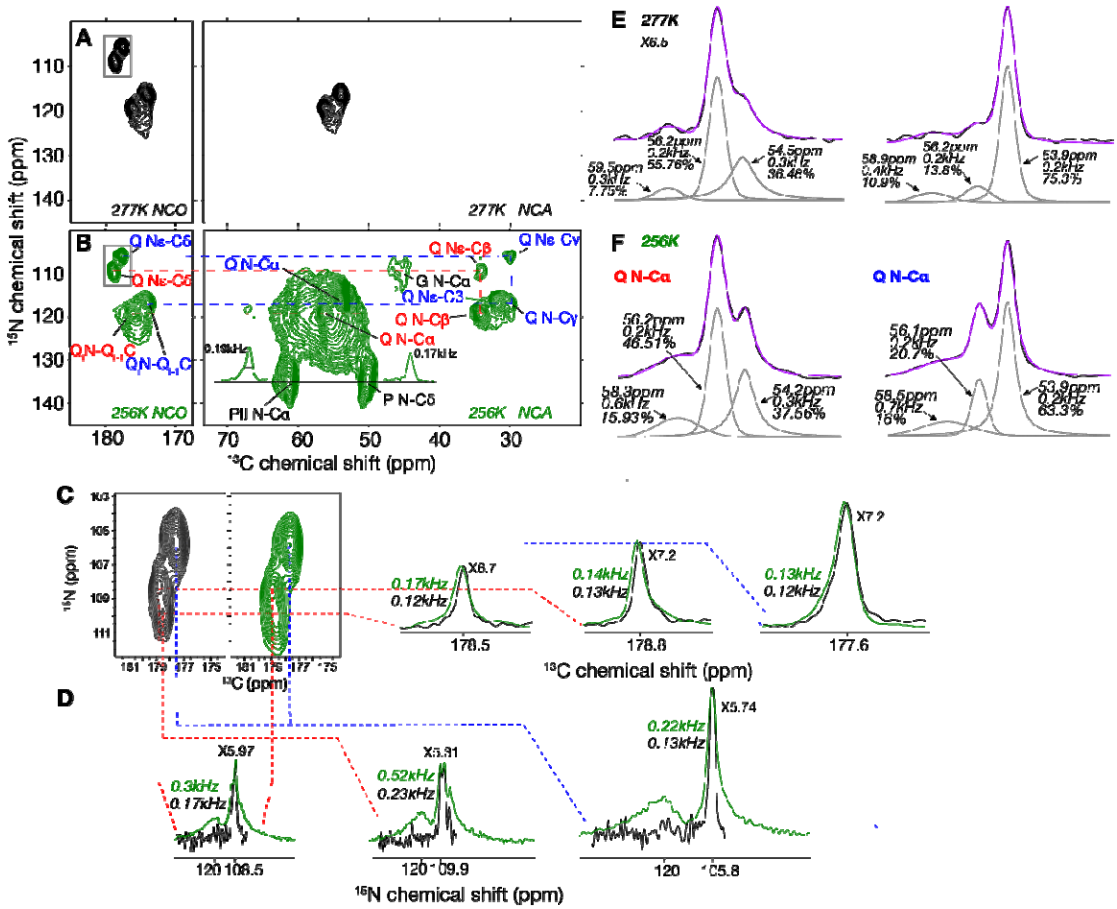

Figure 4. 2D N-C spectra at 277 and 256K. (A) 277K using NCO and NCA pulse sequences and (B) at 256K. (C) Zoomed Q Nε-Cδ connectivities shown in box in panels "A" and "B" at 256K (green) and 277K (black). Their 1D horizontal slices demonstrate small changes in ^{13}C signal widths. (D) 1D vertical slices of panel (C) show larger discrepancies in ^{15}N signal line widths between two temperatures. (E) 1D ^{13}C N-Cα slices of types a and b glutamines at 277K. (F) 1D N-Cα slices of types a and b glutamines at 256K. The signal intensity was increased 6.5 times to reach same intensity as at 256K.

At low temperature, the N-Cα region gained a broad background signal surrounding the narrow backbone peaks of the polyQ core residues (**Figure 4**B). **Figure 4**C,D shows an enlargement of the side chain Nε-Cδ signals of the polyQ core residues at both temperatures. Their 1D slices show small increases in line widths of both glutamine types, for both the ^{13}C and ^{15}N dimensions. The highest increase was observed for type "a" glutamine (from 0.12 to 0.17 kHz for ^{13}C). The modest alterations of signal widths indicate that the glutamine side chains experienced the solvent freezing. 1D slices of backbone signals (N-Cα) are shown in **Figure 4**E,F. At both temperatures, signals were deconvoluted using three peaks. Both Qa and Qb maintain their linewidths at two temperatures indicating that these glutamine backbones are highly ordered in the fiber core and relatively insensitive to the solvent mobility. However, a broad third signal at 59.5ppm (**Figure 4**D) accounts for 7.75% of total integrated Cα signal intensities. At 256K, a broad signal becomes ~16% of the integrated intensity and shifts upfield to 58.3ppm (**Figure 4**C). This region of the spectrum is expected to show signals from most HttEx1 residues except the prolines.

Q44-HttEx1 contains in total 120 residues composed of 31 prolines, 50 glutamine residues, and 39 other residue types. Thus, up to 39 non-polyQ residues could contribute to the broad signals, along with surface-exposed Gln residues in the turn or loop regions of the polyQ domain. However, due to the peak broadness these are impossible to separately identify.

Temperature-dependent changes in dipolar order parameters

We observed (above and before) evidence for glutamine (and other) residues displaying a modest amount of solvent-coupled motion on the surface of the fibril core. Unlike highly flexible residues (visible in INEPT spectra), core-adjacent amino acids appear in CP spectra but have reduced dipolar couplings and short relaxation times due to partial mobility (Hoop et al., 2014). Accordingly, they are difficult to observe, especially if the peaks are close to the dominant peaks of the rigid polyQ core. We next explore an approach for selectively probing such semi-rigid residues, with CP-based ssNMR experiments in which rigid sites are selectively dephased based on their strong ^{1}H-^{13}C dipolar couplings.

The impact of molecular motions that modulate dipolar interactions can be measured via dipolar chemical shift correlation (DIPSHIFT) experiments, yielding dipolar order parameters (Munowitz et al., 1981). Figure 5A illustrates this for simulated ^{13}C-^{1}H dephasing curves where rapid dephasing (under the effect of the ^{1}H-^{13}C dipolar coupling) represents more order (less motion) and slow dephasing indicates increased mobility. The corresponding experimental dephasing curves for Cα-H spin pairs in the Q44-HttEx1 fibrils were measured for unfrozen and frozen fibrils (**Figure 5**B-C). Both types of glutamines in the fiber core showed rapid dephasing (and clear dipolar oscillations) at 277K, indicating a similarly high backbone rigidity even without sample freezing (**Figure 5**B). The obtained data were consistent with prior measurements performed under different conditions or using different fibril types (Hoop et al., 2014; Lin et al., 2017). At 256K, the dephasing was more pronounced, indicating a higher dipolar coupling constant (i.e. less dynamic averaging). Notably, both dephasing curves cross the x-axis (i.e. no residual NMR signal), at either 0.2 or ~0.17ms recoupling time. On the other hand, proline signals show slow dephasing (**Figure 5**D) at 277K indicating increased mobility compared to the amyloid core (low order parameters). In addition, prolines with random coil structure experienced higher mobility than those in the PPII helices. The connection to mobility was confirmed upon freezing the sample, when the Pro dephasing curves resembled those of the rigid amyloid core reached zero signal at 0.14 and 0.16ms for Pro Cδ and ProII Cα respectively (**Figure 5**E). The obtained data provide further support for close connections between solvent dynamics and the segment-specific dynamics of the HttEx1 fibrils, and also paves the way for selectively observing the semi-mobile fibril parts by ssNMR.

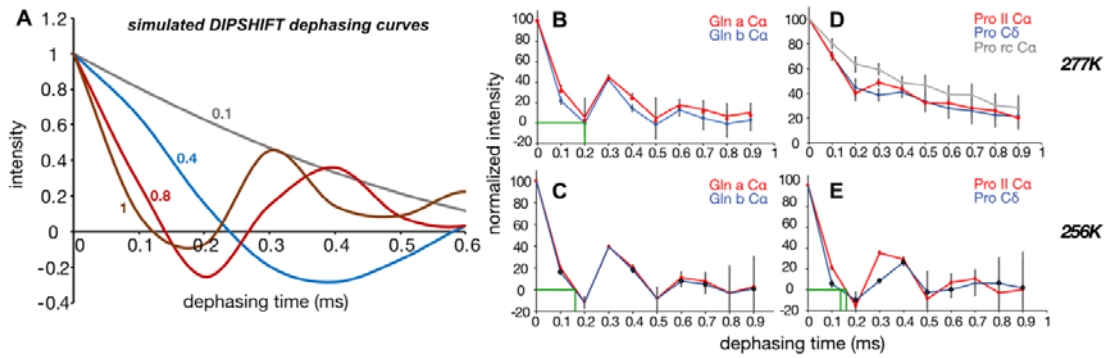

Figure 5. Dipolar dephasing curves for Q44-HttEx1 at variable temperature. (A) Simulated ^{13}Cα-^{1}H dephasing curves based on R18$_1^7$ -based ^{1}H-^{13}C dipolar recoupling, for different order parameter values between 0.1 and 1 and with 0.5ms relaxation (Lin et al., 2017). (B) Experimental dephasing curves of the 'a' and 'b' glutamine types at 277K, and (C) at 256K. (D) Experimental dephasing curves of prolines from PPII helices (red, blue) and from the random coil conformation (grey) at 277K, and (E) at 256K. Experimental data were measured at 600 MHz (^{1}H) and 8 kHz MAS.

Revealing residues with intermediate dynamics

The above data allowed for the design of DYSE-type selective experiments based on the general principles of DYSE spectral editing, as recently reviewed (Matlahov & Wel, 2018). We could use DIPSHIFT dephasing to selectively suppress the normally dominant signals from the fiber core that obscure weak signals from more mobile (surface) residues. As noted above, in the unfrozen sample a dephasing time near 0.2ms caused the most rigid residues to dephase (signal intensity zero or negative) while more mobile (but CP-detected) residues were still observable with positive signal intensity (Figure 5). Thus, by combining CP-based signal generation with ^{1}H-^{13}C DIPSHIFT recoupling one would expect to obtain spectra showing primarily those residues in the protein with intermediate dynamics, yielding an intermediate motion selective (IMS) DYSE experiment. As an example, we combined a DIPSHIFT dephasing block with a canonical ^{13}C-^{13}C DARR pulse sequence (**Figure 6**).

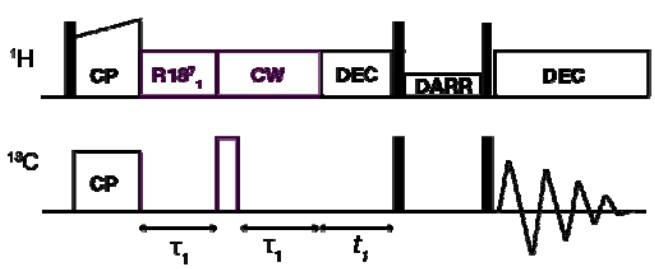

Figure 6. Pulse sequence of combined DIPSHIFT and DARR experiments. After the ramped CP, a DIPSHIFT dipolar filter is applied, with a fixed ^{1}H-^{13}C recoupling period, here shown with R18$_1^7$ recoupling. Subsequently, the residual ^{13}C signal (from non-rigid carbons) is allowed to evolve under incrementing t_1 periods, prior to DARR-based ^{13}C-^{13}C polarization exchange. This pulse sequence generates a broad-band ^{13}C-^{13}C spectrum, but the DIPSHIFT filter would only work fully for the ^{13}C-^{1}H protonated carbons (CH/CH$_2$).

The approach was tested in a DIPSHIFT-filtered 2D ^{13}C-^{13}C DARR spectrum on the Q44-HttEx1 fibrils studied earlier in this report. A normal ^{13}C-^{13}C DARR spectrum without dynamic filtering is shown in **Figure 7**A, whilst the dynamically filtered variant is shown in **Figure 7**B. After 0.2ms of DIPSHIFT filtering, the most rigid residues appeared as negative signals (orange) whereas positive cross-peaks (blue) represent residues that have not been dephased completely. Therefore, these latter signals stem from partly mobile sites, e.g. in the flanking domains and on the fiber surface. Note that the DIPSHIFT experiment (as discussed above) was optimized for dephasing of protonated, immobile aliphatic carbons (in particular C-H groups). Methyl groups and non-protonated carbons (e.g. C=O groups) were not expected to be properly dephased, even in cases where they are part of the rigid structure.

So, here we focused on the signals stemming from relevant carbon sites (e.g. Cα carbons, and non-methyl side chain carbons) along the indirect dimension of the 2D. Off-diagonal peaks involving the polyQ core (type 'a' and 'b') Cα appear as negative peaks, indicating their rigidity. This is true in the aliphatic part of the spectrum as well as the shown Cα-to-C=O cross-peaks. The filtering is applied prior to the t_1 evolution, such that the "filtered" C-H group should be in the indirect dimension of the 2D spectrum. The converse signal (from C=O to Cα; across the diagonal) is not negative in intensity (Figure S5).

The purpose of this experiment was to identify and observe semi-mobile residues. These peaks would manifest as positive off-diagonal peaks (shown in blue) in the chemical shift range of non-methyl aliphatic carbons (70 to 30 ppm on the vertical axis). Indeed, we note several such peaks, with the strongest signals stemming from the proline residues of the PRD (marked P and PPII). These signals had been weak to modest in the normal DARR spectrum (**Figure 7**A), but were prominent in the filtered spectrum. Notably, the 'random coil' Pro signal (Prc) was particularly strong relative to the PPII peak, compared to the normal DARR 2D. This illustrates nicely that the signal intensities are dependent on their molecular dynamics.

We had a particular interest in probing for glutamine residues on the fiber surface, which have chemical shifts similar to those of the rigid buried core. As noted above, partial insight into these residues was reported in prior work, but a detailed study was complicated by the proximity of the dominant rigid core signals. In the filtered spectrum, previously invisible positive glutamine signals now became observable, close to the (orange) filtered signals of the buried core. The signal at 29.9 x 55.46 ppm lines up well with Qc form (**Figure 7**B), previously identified as more dynamic Gln residues (from site-specific labeling studies). Secondary structure analysis indicates a random coil conformation. These chemical shifts of Qc in the full exon 1 resemble the Q47c1 signal site-specifically assigned in residue-specifically labeled $htt^{NT}Q_{30}P_{10}K_2$ Htt N-terminal fragment peptide, reflecting a non-β-strand configuration just outside the amyloid core (Hoop et al., 2014) (**Figure 7**C, Q(near core); Table S3). A second positive signal at 29.0 x 53.3 ppm (coined Qd) represents a distinct glutamine population with chemical shifts indicative of a random coil conformation (**Figure 7**B). These semi-rigid Gln residues likely stem from residues on or near the polyQ amyloid core, either from residues in the β-turn of the Q44 β-hairpin or from the terminal ends of the polyQ domain. A small number of Gln residues is also present in the C-terminal PRD tail, which is typically more visible in INEPT- than in CP-based spectra (Caulkins et al., 2018; Lin et al., 2017).

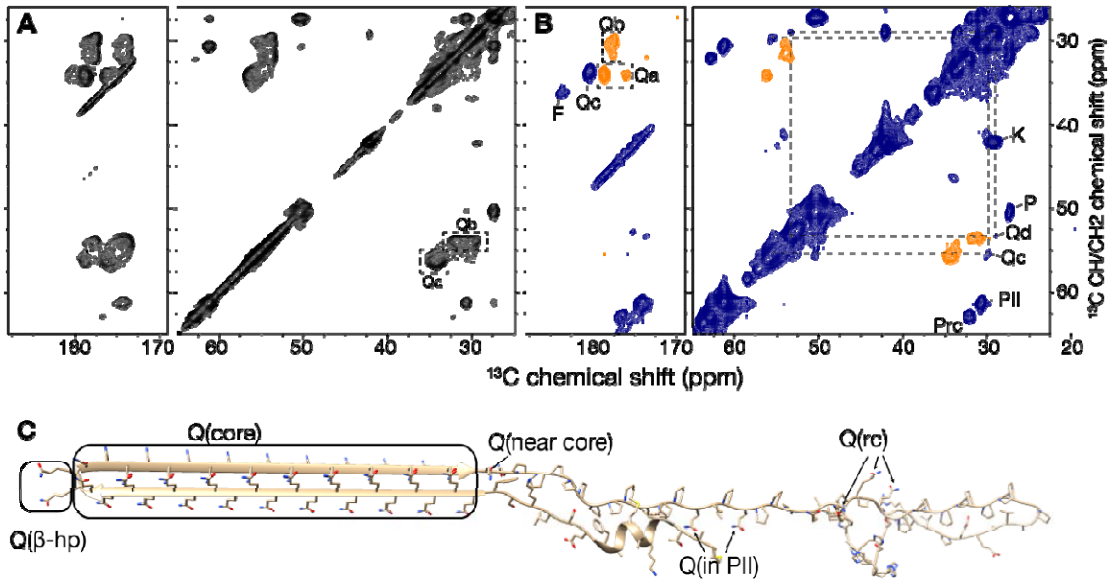

Figure 7. Intermediate-motion selection DYSE in ^{13}C-^{13}C 2D MAS NMR. (A) 2D ^{13}C-^{13}C DARR experiment at 277K. The dominant Cα-Cβ/Cγ peaks of the rigid core signals "Qa" and "Qb" are marked. (B) Corresponding DIPSHIFT-filtered DARR experiment at 277K, using a 0.2ms $R18_1^7$ dipolar recoupling period at 10 kHz MAS. The previously marked rigid core signals now are negative (orange), while previously invisible glutamine signals become visible as positive peaks (blue). These are marked as Qc and Qd. Other strong positive signals from non-Gln residues outside the fiber core are also marked (E, K, P residues). (C) Schematic model of Q44-HttEx1 monomer as present in our model of the Q44-HttEx1 fibril structure, marking the locations of polyQ-domain glutamine residues outside the fiber core. Multiple glutamines in the β-turn are labelled as Q(β-hp) (left), terminal Gln residues at the end of the polyQ segment marked as ("near core"), and a small number of Gln in the PRD indicated as "rc" and "PII".

Discussion

We employed complementary ssNMR experiments to study how protein segments within Q44-HttEx1 fibrils display a range of dynamics. By probing both the solvent (^{1}H MAS NMR) and the protein (^{13}C/^{15}N MAS NMR) we examined the interplay of solvent dynamics and (segmental) protein motion. The ^{1}H NMR revealed the presence of distinct water pools within the hydrated fibril sample. While all water pools in the sample showed a degree of freezing point depression, this effect was more pronounced for one or more of the fibril-associated water pools. Presumably this reflects hydration water that forms a freezing-resistant fluid layer around the protein even when the bulk water is frozen. This finding is reminiscent of prior (ssNMR) studies of hydrated protein crystals, peptide fibrils and liposome samples (Böckmann et al., 2009; Mandal & van der Wel, 2016; Wang et al., 2017). As in other amyloids, there are multiple types of water pools: bulk water, peptide-bound water and strongly bound interfibrillar water. It was previously suggested that water molecules may play a key part in the polymorphic structures in amyloids (Thirumalai et al., 2012), which may also be the case for these Htt protein fibrils.

Our variable-temperature ^{13}C/^{15}N-detected measurements on the protein fibrils themselves showed how changes in the solvent dynamics impacted the mobility of different regions of the HttEx1 fibrils. Segments with a high degree of flexibility are found in the C-terminal tail of the protein, and to a lesser extent in the Htt^{NT} N-terminus. Solvent freezing leads to a loss of flexibility and an extreme broadening of the NMR resonances, which in some cases effectively prohibited visibility. This renders direct studies of these regions (at low temperature) highly difficult. Fortunately, these protein regions are routinely studied using INEPT-based ssNMR approaches that selectively show only highly flexible protein parts. Although not shown in the current work, prior studies have reported extensively on the flexible parts of the C-terminal tail of HttEx1 based on such experiments (Boatz et al., 2020; Caulkins et al., 2018; Isas et al., 2015, 2017; Lin et al., 2017).

The current data provided further support the conclusion that aggregated polyQ segments form a rigid fiber core devoid of water molecules, within which the glutamine backbone and side chain are highly ordered and sequestered. Upon sample freezing, many resonances throughout the protein are broadened, but the impact on the Gln backbone and side chain resonances are very small. This can only be explained by these structural elements being remote from the solvent phase, and insensitive to its mobility. This observation is well explained by our previously published structural model of the polyQ core of these HttEx1 fibrils, reproduced in Figure 1A (Boatz et al., 2020). This model was derived from an integrative structural biology approach combining a diversity of EM, X-ray diffraction and ssNMR data. It shows a fiber core containing approximately nice interdigitating β-sheets, placing the Gln side chains in a constrained steric-zipper arrangement. In this core structure, a large majority of the Gln residues is placed in the fiber core, with only 19 % of the polyQ domain placed at the fiber surface.

Yet, it is these glutamine residues on the fiber surface that are of significant interest. On the one hand, they include the as-yet poorly understood β-turn regions of the β-hairpins of polyQ-expanded HttEx1 fibrils (Hoop et al., 2016; Matlahov & Wel, 2019). Secondarily, the outer surface of the fibers features the surface grooves that are characteristic of amyloid-like fibrils, and feature the binding sites of both amyloid-specific fluorescent dyes and other diagnostic tracer molecules (Bertoglio et al., 2021; Biancalana

& Koide, 2010; Fändrich et al., 2018; Schütz et al., 2011). Yet, these solvent-facing glutamine residues are hard to distinguish from those internal to the polyQ core, with the latter dominating the CP-based 1D and 2D ssNMR spectra. Nonetheless, upon sample freezing we observed changes in signal intensity, linewidth and dipolar order parameters also affecting (though modestly) the signals from the polyQ domain. This could stem from residual dynamics within the core, or may also be due to the signals from surface-facing glutamine amino acids. However, the variable temperature spectra failed to give much insight into their resonance frequencies or dynamic properties. The freezing out of the more flexible amino acid segments elsewhere in the protein dominates the spectra and masks any new signals from the Gln residues (e.g. **Figure 4**). Highly broadened signals arose that likely stem largely from the htt^{NT} and PRD segments, which are almost (Sivanandam et al., 2011) entirely devoid of β-sheet structure and are solvent exposed and dynamic. The obtained data reinforces previously reported conclusions regarding the notable range of dynamics seen in HttEx1 fibrils. For instance, the variable-temperature order parameter measurements (**Figure 5**) show that solvent freezing has a small ordering effect on the Gln signals, but causes a dramatic change for the PRD segments. We previously reported similar findings contrasting the motions of site-specifically labeled residues in the polyQ and Htt^{NT} segments of Htt N-terminal fragment peptide fibrils (Hoop et al., 2014), but this is the first report of such measurements applied to Q44-HttEx1 fibrils.

An important aspect of the current study is the introduction of a (to the best of our knowledge) new approach to DYSE ssNMR, which is focused on observing signals from residues with a mobility in-between highly rigid and highly flexible. A similar technique was recently reported using a different approach via ^{13}C-^{15}N REDOR filtering to selectively observe protein signals displaying ms time scale motion (Kashefi et al., 2019). In our approach, we integrated a DIPSHIFT-based filtering element in a standard CP-ssNMR pulse sequence, to selectively dephase the signals from rigid protein segments, thus highlighting the signals from semi-rigid residues. We show how this approach allows us to observe previously invisible cross-peaks from surface-facing residues on the polyQ core, which in normal spectra are overwhelmed by nearby high-intensity signals from the polyQ core internal structure. The observed resonances reveal two surface-facing types of Gln residue types, with chemical shifts summarized in Table S3. Whilst one residue type matches prior studies, the other (type "d") appears to be a novel type of glutamine on the fiber core surface. Though distinct from each other, both Gln residue types have chemical shifts that are inconsistent with β-sheet structure, as expected for non-amyloid-core residues. A further characterization of the structural features of these residues requires further studies, which are ongoing.

The use of the dipolar-filter to selectively suppress signals from rigid components, in order to observe semi-rigid sample components via CP-based ssNMR, could be extended to other types of ssNMR experiments. As noted, the described integration with a broadband technique such as the employed DARR ^{13}C-^{13}C 2D spectrum works, but one needs to keep in mind that it designed specifically for non-methyl protonated aliphatic carbons (CH, CH_2 groups). This suggests that an attractive use may be to integrate it into Cα-selective experiments, such as NCA(CX) pulse sequences. However, as discussed around **Figure 4**, a caveat with such an approach is that such DCP experiments inherently limit the recovery of signals from (semi) mobile residues. A workaround for this issue could involve the use of a (frequency selective) TEDOR pulse program to measure the equivalent of an NCA experiment (Daviso et al., 2013) with

intermediate mobility selection (IMS-DYSE). Other variations and implementations could be envisioned, for instance toward applications at fast MAS, alternative ^{1}H-^{13}C recoupling techniques, etc.

The current work provides new insights into the complex dynamics of HttEx1 fibrils, which feature dynamics spanning from highly rigid to highly flexible, for the fibril core and flanking domains. This is a feature common to many pathogenic protein fibrils, including tau and α-synuclein (Andronesi et al., 2008; Fitzpatrick et al., 2017; Helmus et al., 2008, 2010; Tuttle et al., 2016). The dynamically disordered flanking domains are biologically interesting as they appear to be target sites for disaggregating chaperones and impact fiber toxicity and polymorphism (Chongtham et al., 2020; Duennwald et al., 2006; Lin et al., 2017; Robertson et al., 2010; Wentink et al., 2020). Beyond reinforcing our understanding of the flexible flanking domain segments, the current work also reveals the signals of mobile Gln residues proximal to the fiber core, which itself is highly rigid and devoid of water. The latter feature is now seen as a common feature of amyloid fibrils (Kloepper et al., 2007), but it does argue against proposed models of nanotubular fibril architectures previously invoked for polyQ fibers (Côté et al., 2012; Laghaei & Mousseau, 2010). Rather, our observations strongly support the idea that the polyQ amyloid core has a block-like architecture in which a large proportion of the Gln residues is buried in the core and inaccessible to water molecules, let alone polyQ-binding antibodies (Boatz et al., 2020; Schneider et al., 2011; Sharma et al., 2005). Nonetheless, through IMS-DYSE and variable temperature studies we obtained direct evidence of the minor population of more mobile Gln residues on the fiber core surface. It is these surface-facing sites that are accessible to the solvent, and thus rendered partly mobile, though not flexible. Although surface-exposed, these partly-immobilized Gln residues are too densely packed (and/or incorrectly structured) for efficient binding by typical polyQ-binding antibodies (F. A. C. Klein et al., 2013; Legleiter et al., 2009; Lin et al., 2017). Still, they are likely implicated in forming part of the surface features of mutant HttEx1 species that are recognized by fluorescent dyes (e.g. ThT), PET ligands, and certain types of HttEx1 aggregation inhibitors (Bertoglio et al., 2021; Kar et al., 2017; Matsuoka et al., 2012; Minakawa & Nagai, 2021).

We envision useful applications of IMS-DYSE experiments beyond amyloid fibrils. In many functional proteins, loops, turns and even whole (enzymatic) domains undergo millisecond timescale motion that may be essential for protein function. Such structural re-arrangements of active sites depend on interactions with water molecules, with hydration and motion being essential for protein function (A. Klein et al., 2021; Singh et al., 2019; Vasa et al., 2019). This applies to many proteins studied by ssNMR, including crystalline globular proteins, large protein complexes, and membrane proteins (Eddy et al., 2015; Kashefi et al., 2019; Saurel et al., 2017). NMR signals from enzymatic active sites (if overlapped) and membrane proteins can be a target for applying such DIPSHIFT-based filtering technique.

Conclusions

We employed complementary methods in ssNMR to study the dynamics of Q44-HttEx1 fibrils, focusing on segments or residues near the rigid fiber core, which have previously remained invisible or only tangentially observed. The mobility was shown to be strongly correlated to the dynamics of the

fiber-associated water pools, in which protein-bound waters resist freezing, but ultimately freeze out the dynamics of flexible regions into static disorder. Variable temperature studies reveal the presence of dynamic components, due to signal broadening and increases in dipolar order parameters, but fail to give detailed insights due to the excessive signal overlap. As a work-around we described and applied a new ^{1}H-^{13}C DIPSHIFT-based dynamic-based spectral editing experiment that suppresses signals from the rigid core, and emphasizes instead those CP-visible signals of partly dynamic core-proximal protein segments. This technique revealed two types of surface-facing glutamines Qc and Qd despite a large excess of rigid polyQ core signals. These results pave the way for further investigations of the fiber surface, with potential implications for diagnostic and inhibitor developments relevant to HD. Moreover, we anticipate similar methods to be useful to a variety of other protein fibrils, membrane proteins, and (bio)materials with surface-facing chemical groups on a more rigid core. For instance, IMS-DYSE measurements could enhance ssNMR studies of nanoparticles, nanomaterials, thin films and bottlebrush polymers (Golkaram et al., 2019; Gruschwitz et al., 2020; Protesescu et al., 2014; Walsh & Knecht, 2017).

Acknowledgements

This work was supported by the National Institutes of Health (grants R01 GM112678 and R01 GM113908 to PvdW; T32 GM088119 to J.C.B), the Achievement Rewards for College Scientists (ARCS) Foundation (J.C.B.), the CHDI Foundation, and the CampagneTeam Huntington foundation.

Bibliography

Andronesi, O. C., von Bergen, M., Biernat, J., Seidel, K., Griesinger, C., Mandelkow, E., & Baldus, M. (2008). Characterization of Alzheimer's-like paired helical filaments from the core domain of tau protein using solid-state NMR spectroscopy. *J Am Chem Soc*, *130*(18), 5922–5928. https://doi.org/10.1021/ja7100517

Bates, G. P., Dorsey, R., Gusella, J. F., Hayden, M. R., Kay, C., Leavitt, B. R., Nance, M., Ross, C. A., Scahill, R. I., Wetzel, R., Wild, E. J., & Tabrizi, S. J. (2015). Huntington disease. *Nature Reviews Disease Primers*, *1*, 15005. https://doi.org/10.1038/nrdp.2015.5

Bäuerlein, F. J. B., Saha, I., Mishra, A., Kalemanov, M., Martínez-Sánchez, A., Klein, R., Dudanova, I., Hipp, M. S., Hartl, F. U., Baumeister, W., & Fernández-Busnadiego, R. (2017). In Situ Architecture and Cellular Interactions of PolyQ Inclusions. *Cell*, 1–20. https://doi.org/10.1016/j.cell.2017.08.009

Bennett, A. E., Rienstra, C. M., Auger, M., Lakshmi, K. V., & Griffin, R. G. (1995). Heteronuclear decoupling in rotating solids. *J Chem Phys*, *103*(16), 6951–6958.

Bertoglio, D., Bard, J., Hessmann, M., Liu, L., Gärtner, A., Lombaerde, S. D., Huscher, B., Zajicek, F., Miranda, A., Peters, F., Herrmann, F., Schaertl, S., Vasilkovska, T., Brown, C. J., Johnson, P. D., Prime, M. E., Mills, M. R., Van der Linden, A., Mrzljak, L., … Munoz-Sanjuan, I. (2021). *A novel imaging ligand as a biomarker for mutant huntingtin-lowering in Huntington's disease* [Preprint]. Neuroscience. https://doi.org/10.1101/2021.07.09.451725

Biancalana, M., & Koide, S. (2010). Molecular mechanism of Thioflavin-T binding to amyloid fibrils. *Biochim. Biophys. Acta*, *1804*(7), 1405–1412. https://doi.org/10.1016/j.bbapap.2010.04.001

Boatz, J. C., Piretra, T., Lasorsa, A., Matlahov, I., Conway, J. F., & van der Wel, P. C. A. (2020). Protofilament Structure and Supramolecular Polymorphism of Aggregated Mutant Huntingtin Exon 1. *Journal of Molecular Biology*, *432*(16), 4722–4744. https://doi.org/10.1016/j.jmb.2020.06.021

Böckmann, A., Gardiennet, C., Verel, R., Hunkeler, A., Loquet, A., Pintacuda, G., Emsley, L., Meier, B. H., & Lesage, A. (2009). Characterization of different water pools in

solid-state NMR protein samples. *J Biomol NMR*, *45*(3), 319–327. https://doi.org/10.1007/s10858-009-9374-3

Bugg, C. W., Isas, J. M., Fischer, T., Patterson, P. H., & Langen, R. (2012). Structural Features and Domain Organization of Huntingtin Fibrils. *J Biol Chem*, *287*(38), 31739–31746. https://doi.org/10.1074/jbc.M112.353839

Caulkins, B. G., Cervantes, S. A., Isas, J. M., & Siemer, A. B. (2018). Dynamics of the Proline-Rich C-Terminus of Huntingtin Exon-1 Fibrils. *The Journal of Physical Chemistry B*, *122*(41), 9507–9515. https://doi.org/10.1021/acs.jpcb.8b09213

Chiti, F., & Dobson, C. M. (2017). Protein Misfolding, Amyloid Formation, and Human Disease: A Summary of Progress Over the Last Decade. *Annu Rev Biochem*, *86*(1), 27–68. https://doi.org/10.1146/annurev-biochem-061516-045115

Chongtham, A., Bornemann, D. J., Barbaro, B. A., Lukacsovich, T., Agrawal, N., Syed, A., Worthge, S., Purcell, J., Burke, J., Chin, T. M., & Marsh, J. L. (2020). Effects of flanking sequences and cellular context on subcellular behavior and pathology of mutant HTT. *Hum Mol Genet*. https://doi.org/10.1093/hmg/ddaa001

Côté, S., Wei, G., & Mousseau, N. (2012). All-Atom Stability and Oligomerization Simulations of Polyglutamine Nanotubes with and without the 17-Amino-Acid N-Terminal Fragment of the Huntingtin Protein. *J Phys Chem B*, *116*(40), 12168–12179. https://doi.org/10.1021/jp306661c

Daviso, E., Eddy, M. T., Andreas, L. B., Griffin, R. G., & Herzfeld, J. (2013). Efficient resonance assignment of proteins in MAS NMR by simultaneous intra- and

inter-residue 3D correlation spectroscopy. *J Biomol NMR*, *55*(3), 257–265. https://doi.org/10.1007/s10858-013-9707-0

Duennwald, M. L., Jagadish, S., Muchowski, P. J., & Lindquist, S. L. (2006). Flanking sequences profoundly alter polyglutamine toxicity in yeast. *Proc. Natl. Acad. Sci. USA*, *103*(29), 11045–11050. https://doi.org/10.1073/pnas.0604547103

Duim, W. C., Jiang, Y., Shen, K., Frydman, J., & Moerner, W. E. (2014). Super-resolution fluorescence of huntingtin reveals growth of globular species into short fibers and coexistence of distinct aggregates. *ACS Chem Biol*, *9*(12), 2767–2778. https://doi.org/10.1021/cb500335w

Eddy, M. T., Su, Y., Silvers, R., Andreas, L., Clark, L., Wagner, G., Pintacuda, G., Emsley, L., & Griffin, R. G. (2015). Lipid bilayer-bound conformation of an integral membrane beta barrel protein by multidimensional MAS NMR. *Journal of Biomolecular NMR*, *61*(3), 299–310. https://doi.org/10.1007/s10858-015-9903-1

El Hariri El Nokab, M., Lasorsa, A., Sebakhy, K. O., Picchioni, F., & van der Wel, P. C. A. (2022). Solid-state NMR spectroscopy insights for resolving different water pools in alginate hydrogels. *Food Hydrocolloids*, 107500. https://doi.org/10.1016/j.foodhyd.2022.107500

Falk, A. S., Bravo-Arredondo, J. M., Varkey, J., Pacheco, S., Langen, R., & Siemer, A. B. (2020). Structural Model of the Proline-Rich Domain of Huntingtin Exon-1 Fibrils. *Biophysical Journal*, *119*(10), 2019–2028. https://doi.org/10.1016/j.bpj.2020.10.010

Fändrich, M., Nyström, S., Nilsson, K. P. R., Böckmann, A., LeVine, H., & Hammarström, P. (2018). Amyloid fibril polymorphism: A challenge for molecular imaging and

therapy. *Journal of Internal Medicine*, *283*(3), 218–237. https://doi.org/10.1111/joim.12732

Fitzpatrick, A. W. P., Falcon, B., He, S., Murzin, A. G., Murshudov, G., Garringer, H. J., Crowther, R. A., Ghetti, B., Goedert, M., & Scheres, S. H. W. (2017). Cryo-EM structures of tau filaments from Alzheimer's disease. *Nature*, *547*(7662), 185–190. https://doi.org/10.1038/nature23002

Fitzpatrick, A. W. P., & Saibil, H. R. (2019). Cryo-EM of amyloid fibrils and cellular aggregates. *Current Opinion in Structural Biology*, *58*, 34–42. https://doi.org/10.1016/j.sbi.2019.05.003

Fowler, D. M., Koulov, A. V., Balch, W. E., & Kelly, J. W. (2007). Functional amyloid—From bacteria to humans. *Trends Biochem Sci*, *32*(5), 217–224. https://doi.org/10.1016/j.tibs.2007.03.003

Galaz-Montoya, J. G., Shahmoradian, S. H., Shen, K., Frydman, J., & Chiu, W. (2021). Cryo-electron tomography provides topological insights into mutant huntingtin exon 1 and polyQ aggregates. *Communications Biology*, *4*(1), 849. https://doi.org/10.1038/s42003-021-02360-2

Gasteiger, E. (2003). ExPASy: The proteomics server for in-depth protein knowledge and analysis. *Nucleic Acids Research*, *31*(13), 3784–3788. https://doi.org/10.1093/nar/gkg563

Golkaram, M., Boetje, L., Dong, J., Suarez, L. E. A., Fodor, C., Maniar, D., van Ruymbeke, E., Faraji, S., Portale, G., & Loos, K. (2019). Supramolecular Mimic for Bottlebrush

Polymers in Bulk. *ACS Omega*, *4*(15), 16481–16492. https://doi.org/10.1021/acsomega.9b02126

Gruschwitz, F. V., Klein, T., Catrouillet, S., & Brendel, J. C. (2020). Supramolecular polymer bottlebrushes. *Chemical Communications*, *56*(38), 5079–5110. https://doi.org/10.1039/D0CC01202E

Guo, Q., Huang, B., Cheng, J., Seefelder, M., Engler, T., Pfeifer, G., Oeckl, P., Otto, M., Moser, F., Maurer, M., Pautsch, A., Baumeister, W., Fernández-Busnadiego, R., & Kochanek, S. (2018). The cryo-electron microscopy structure of huntingtin. *Nature*, *555*(7694), 117–120. https://doi.org/10.1038/nature25502

Harris, R. K., Becker, E. D., De Menezes, S. M. C., Granger, P., Hoffman, R. E., & Zilm, K. W. (2008). Further conventions for NMR shielding and chemical shifts (IUPAC Recommendations 2008). *Magn Reson Chem*, *46*(6), 582–598. https://doi.org/10.1002/mrc.2225

Helmus, J. J., Surewicz, K., Nadaud, P. S., Surewicz, W. K., & Jaroniec, C. P. (2008). Molecular conformation and dynamics of the Y145Stop variant of human prion protein in amyloid fibrils. *Proceedings of the National Academy of Sciences*, *105*(17), 6284–6289. https://doi.org/10.1073/pnas.0711716105

Helmus, J. J., Surewicz, K., Surewicz, W. K., & Jaroniec, C. P. (2010). Conformational Flexibility of Y145Stop Human Prion Protein Amyloid Fibrils Probed by Solid-State Nuclear Magnetic Resonance Spectroscopy. *Journal of the American Chemical Society*, *132*(7), 2393–2403. https://doi.org/10.1021/ja909827v

Hervas, R., Rau, M. J., Park, Y., Zhang, W., Murzin, A. G., Fitzpatrick, J. A. J., Scheres, S. H. W., & Si, K. (2020). Cryo-EM structure of a neuronal functional amyloid implicated in memory persistence in *Drosophila*. *Science*, *367*(6483), 1230–1234. https://doi.org/10.1126/science.aba3526

Hoop, C. L., Lin, H.-K., Kar, K., Hou, Z., Poirier, M. A., Wetzel, R., & Wel, P. C. A. van der. (2014). Polyglutamine Amyloid Core Boundaries and Flanking Domain Dynamics in Huntingtin Fragment Fibrils Determined by Solid-State Nuclear Magnetic Resonance. *Biochemistry*, *53*(42), 6653–6666. https://doi.org/10.1021/bi501010q

Hoop, C. L., Lin, H.-K., Kar, K., Magyarfalvi, G., Lamley, J. M., Boatz, J. C., Mandal, A., Lewandowski, J. R., Wetzel, R., & Wel, P. C. A. van der. (2016). Huntingtin exon 1 fibrils feature an interdigitated β-hairpin–based polyglutamine core. *Proceedings of the National Academy of Sciences*, *113*(6), 1546–1551. https://doi.org/10.1073/pnas.1521933113

Isas, J. M., Langen, A., Isas, M. C., Pandey, N. K., & Siemer, A. B. (2017). Formation and Structure of Wild Type Huntingtin Exon-1 Fibrils. *Biochemistry*, *56*(28), 3579–3586. https://doi.org/10.1021/acs.biochem.7b00138

Isas, J. M., Langen, R., & Siemer, A. B. (2015). Solid-State Nuclear Magnetic Resonance on the Static and Dynamic Domains of Huntingtin Exon-1 Fibrils. *Biochemistry*, *54*(25), 3942–3949. https://doi.org/10.1021/acs.biochem.5b00281

Isas, J. M., Pandey, N. K., Teranishi, K., Okada, A. K., Applebaum, A., Meier, F., Langen, R., & Siemer, A. B. (2019). *Huntingtin fibrils with different toxicity, structure, and*

seeding potential can be reversibly interconverted (p. 703769). bioRxiv. https://doi.org/10.1101/703769

Kar, K., Baker, M. A., Lengyel, G. A., Hoop, C. L., Kodali, R., Byeon, I.-J., Horne, W. S., van der Wel, P. C. A., & Wetzel, R. (2017). Backbone Engineering within a Latent β-Hairpin Structure to Design Inhibitors of Polyglutamine Amyloid Formation. *J Mol Biol*, *429*(2), 308–323. https://doi.org/10.1016/j.jmb.2016.12.010

Kashefi, M., Malik, N., Struppe, J. O., & Thompson, L. K. (2019). Carbon-nitrogen REDOR to identify ms-timescale mobility in proteins. *J Magn Reson*. https://doi.org/10.1016/j.jmr.2019.05.008

Khoshnan, A., Ko, J., & Patterson, P. H. (2002). Effects of intracellular expression of anti-huntingtin antibodies of various specificities on mutant huntingtin aggregation and toxicity. *Proceedings of the National Academy of Sciences*, *99*(2), 1002–1007. https://doi.org/10.1073/pnas.022631799

Klein, A., Rovó, P., Sakhrani, V. V., Wang, Y., Holmes, J., Liu, V., Skowronek, P., Kukuk, L., Vasa, S. K., Güntert, P., Mueller, L. J., & Linser, R. (2021). *Residue-specific insights into (2x)72 kDa tryptophan synthase obtained from fast-MAS 1H-detected solid-state NMR* (p. 2021.05.12.443859). bioRxiv. https://doi.org/10.1101/2021.05.12.443859

Klein, F. A. C., Zeder-Lutz, G., Cousido-Siah, A., Mitschler, A., Katz, A., Eberling, P., Mandel, J.-L., Podjarny, A., & Trottier, Y. (2013). Linear and extended: A common polyglutamine conformation recognized by the three antibodies MW1, 1C2 and 3B5H10. *Hum Mol Genet*, *22*(20), 4215–4223. https://doi.org/10.1093/hmg/ddt273

Kloepper, K. D., Hartman, K. L., Ladror, D. T., & Rienstra, C. M. (2007). Solid-State NMR Spectroscopy Reveals That Water Is Nonessential to the Core Structure of α-Synuclein Fibrils. *J Phys Chem B*, *111*(47), 13353–13356. https://doi.org/10.1021/jp077036z

Laghaei, R., & Mousseau, N. (2010). Spontaneous formation of polyglutamine nanotubes with molecular dynamics simulations. *J Chem Phys*, *132*(16), 165102. https://doi.org/10.1063/1.3383244

Legleiter, J., Lotz, G. P., Miller, J., Ko, J., Ng, C., Williams, G. L., Finkbeiner, S., Patterson, P. H., & Muchowski, P. J. (2009). Monoclonal Antibodies Recognize Distinct Conformational Epitopes Formed by Polyglutamine in a Mutant Huntingtin Fragment*. *Journal of Biological Chemistry*, *284*(32), 21647–21658. https://doi.org/10.1074/jbc.M109.016923

Lin, H.-K., Boatz, J. C., Krabbendam, I. E., Kodali, R., Hou, Z., Wetzel, R., Dolga, A. M., Poirier, M. A., & Wel, P. C. A. van der. (2017). Fibril polymorphism affects immobilized non-amyloid flanking domains of huntingtin exon1 rather than its polyglutamine core. *Nature Communications*, *8*, 15462. https://doi.org/10.1038/ncomms15462

Liu, L., Prime, M. E., Lee, M. R., Khetarpal, V., Brown, C. J., Johnson, P. D., Azpiazu, P., Chen, A., Clark-Frew, D., Coe, S., Davis, R., Dickie, A., Ebneth, A., Esposito, S., Gadouleau, E., Gai, X., Galan, S., Green, S., Greenaway, C., … Dominguez, C. (2020). Imaging Mutant Huntingtin Aggregates: Development of a Potential PET

ligand. *Journal of Medicinal Chemistry*, *63*(15), 8608–8633. https://doi.org/10.1021/acs.jmedchem.0c00955

Lutter, L., Aubrey, L. D., & Xue, W.-F. (2021). On the Structural Diversity and Individuality of Polymorphic Amyloid Protein Assemblies. *Journal of Molecular Biology*, *433*(20), 167124. https://doi.org/10.1016/j.jmb.2021.167124

Macdonald, M. (1993). A novel gene containing a trinucleotide repeat that is expanded and unstable on Huntington's disease chromosomes. *Cell*, *72*(6), 971–983. https://doi.org/10.1016/0092-8674(93)90585-E

Mandal, A., Boatz, J. C., Wheeler, T. B., & Wel, P. C. A. van der. (2017). On the use of ultracentrifugal devices for routine sample preparation in biomolecular magic-angle-spinning NMR. *Journal of Biomolecular Nmr*, *67*(3), 165–178. https://doi.org/10.1007/s10858-017-0089-6

Mandal, A., Hoop, C. L., DeLucia, M., Kodali, R., Kagan, V. E., Ahn, J., & van der Wel, P. C. A. (2015). Structural Changes and Proapoptotic Peroxidase Activity of Cardiolipin-Bound Mitochondrial Cytochrome c. *Biophys. J.*, *109*(9), 1873–1884. https://doi.org/10.1016/j.bpj.2015.09.016

Mandal, A., & van der Wel, P. C. A. (2016). MAS 1H NMR Probes Freezing Point Depression of Water and Liquid-Gel Phase Transitions in Liposomes. *Biophysical Journal*, *111*(9), 1965–1973. https://doi.org/10.1016/j.bpj.2016.09.027

Matlahov, I., & Wel, P. C. van der. (2019). Conformational studies of pathogenic expanded polyglutamine protein deposits from Huntington's disease. *Experimental Biology and Medicine*, *244*(17), 1584–1595. https://doi.org/10.1177/1535370219856620

Matlahov, I., & Wel, P. C. A. van der. (2018). Hidden motions and motion-induced invisibility: Dynamics-based spectral editing in solid-state NMR. *Methods (San Diego, Calif.)*. https://doi.org/10.1016/j.ymeth.2018.04.015

Matsuoka, S., Murai, M., Yamazaki, T., & Inoue, M. (2012). Short polyglutamine peptide forms a high-affinity binding site for thioflavin-T at the N-terminus. *Organic & Biomolecular Chemistry*, *10*(30), 5787. https://doi.org/10.1039/c2ob07157f

Minakawa, E. N., & Nagai, Y. (2021). Protein Aggregation Inhibitors as Disease-Modifying Therapies for Polyglutamine Diseases. *Frontiers in Neuroscience*, *15*, 621996. https://doi.org/10.3389/fnins.2021.621996

Morcombe, C. R., & Zilm, K. W. (2003). Chemical shift referencing in MAS solid state NMR. *J Magn Reson*, *162*(2), 479–486. https://doi.org/10.1016/S1090-7807(03)00082-X

Muiznieks, L. D., Sharpe, S., Pomès, R., & Keeley, F. W. (2018). Role of Liquid–Liquid Phase Separation in Assembly of Elastin and Other Extracellular Matrix Proteins. *Journal of Molecular Biology*, *430*(23), 4741–4753. https://doi.org/10.1016/j.jmb.2018.06.010

Munowitz, M. G., Griffin, R. G., Bodenhausen, G., & Huang, T. H. (1981). Two-dimensional rotational spin-echo nuclear magnetic resonance in solids: Correlation of chemical shift and dipolar interactions. *Journal of the American Chemical Society*, *103*(10), 2529–2533. https://doi.org/10.1021/ja00400a007

Murray, D. T., Kato, M., Lin, Y., Thurber, K. R., Hung, I., McKnight, S. L., & Tycko, R. (2017). Structure of FUS Protein Fibrils and Its Relevance to Self-Assembly and

Phase Separation of Low-Complexity Domains. *Cell*, *171*(3), 615-627.e16. https://doi.org/10.1016/j.cell.2017.08.048

Protesescu, L., Rossini, A. J., Kriegner, D., Valla, M., de Kergommeaux, A., Walter, M., Kravchyk, K. V., Nachtegaal, M., Stangl, J., Malaman, B., Reiss, P., Lesage, A., Emsley, L., Copéret, C., & Kovalenko, M. V. (2014). Unraveling the core-shell structure of ligand-capped Sn/SnOx nanoparticles by surface-enhanced nuclear magnetic resonance, Mössbauer, and X-ray absorption spectroscopies. *ACS Nano*, *8*(3), 2639–2648. https://doi.org/10.1021/nn406344n

Robertson, A. L., Headey, S. J., Saunders, H. M., Ecroyd, H., Scanlon, M. J., Carver, J. A., & Bottomley, S. P. (2010). Small heat-shock proteins interact with a flanking domain to suppress polyglutamine aggregation. *Proc. Natl. Acad. Sci. USA*, *107*(23), 10424–10429. https://doi.org/10.1073/pnas.0914773107

Ryder, B. D., Matlahov, I., Bali, S., Vaquer-Alicea, J., van der Wel, P. C. A., & Joachimiak, L. A. (2021). Regulatory inter-domain interactions influence Hsp70 recruitment to the DnaJB8 chaperone. *Nature Communications*, *12*(1), 946. https://doi.org/10.1038/s41467-021-21147-x

Saurel, O., Iordanov, I., Nars, G., Demange, P., Le Marchand, T., Andreas, L. B., Pintacuda, G., & Milon, A. (2017). Local and Global Dynamics in Klebsiella pneumoniae Outer Membrane Protein a in Lipid Bilayers Probed at Atomic Resolution. *J Am Chem Soc*, *139*(4), 1590–1597. https://doi.org/10.1021/jacs.6b11565

Scherzinger, E., Lurz, R., Turmaine, M., Mangiarini, L., Hollenbach, B., Hasenbank, R., Bates, G. P., Davies, S. W., Lehrach, H., & Wanker, E. E. (1997).

Huntingtin-Encoded Polyglutamine Expansions Form Amyloid-like Protein Aggregates In Vitro and In Vivo. *Cell*, *90*(3), 549–558. https://doi.org/10.1016/S0092-8674(00)80514-0

Schmidt, J., Hoffmann, A., Spiess, H. W., & Sebastiani, D. (2006). Bulk Chemical Shifts in Hydrogen-Bonded Systems from First-Principles Calculations and Solid-State-NMR. *The Journal of Physical Chemistry B*, *110*(46), 23204–23210. https://doi.org/10.1021/jp0640732

Schneider, R., Schumacher, M. C., Mueller, H., Nand, D., Klaukien, V., Heise, H., Riedel, D., Wolf, G., Behrmann, E., Raunser, S., Seidel, R., Engelhard, M., & Baldus, M. (2011). Structural characterization of polyglutamine fibrils by solid-state NMR spectroscopy. *J Mol Biol*, *412*(1), 121–136. https://doi.org/10.1016/j.jmb.2011.06.045

Schütz, A. K., Soragni, A., Hornemann, S., Aguzzi, A., Ernst, M., Böckmann, A., & Meier, B. H. (2011). The Amyloid–Congo Red Interface at Atomic Resolution. *Angew. Chem. Int. Ed.*, *50*(26), 5956–5960. https://doi.org/10.1002/anie.201008276

Sharma, D., Shinchuk, L. M., Inouye, H., Wetzel, R., & Kirschner, D. A. (2005). Polyglutamine homopolymers having 8-45 residues form slablike beta-crystallite assemblies. *Proteins*, *61*(2), 398–411. https://doi.org/10.1002/prot.20602

Singh, H., Vasa, S. K., Jangra, H., Rovó, P., Päslack, C., Das, C. K., Zipse, H., Schäfer, L. V., & Linser, R. (2019). Fast Microsecond Dynamics of the Protein–Water Network in the Active Site of Human Carbonic Anhydrase II Studied by Solid-State NMR

Spectroscopy. *Journal of the American Chemical Society*, *141*(49), 19276–19288. https://doi.org/10.1021/jacs.9b05311

Sivanandam, V. N., Jayaraman, M., Hoop, C. L., Kodali, R., Wetzel, R., & Wel, P. C. A. van der. (2011). The aggregation-enhancing huntingtin N-terminus is helical in amyloid fibrils. *Journal of the American Chemical Society*, *133*(12), 4558–4566. https://doi.org/10.1021/ja110715f

Skinner, S. P., Fogh, R. H., Boucher, W., Ragan, T. J., Mureddu, L. G., & Vuister, G. W. (2016). CcpNmr AnalysisAssign: A flexible platform for integrated NMR analysis. *J Biomol NMR*, *66*(2), 111–124. https://doi.org/10.1007/s10858-016-0060-y

Southwell, A. L., Khoshnan, A., Dunn, D. E., Bugg, C. W., Lo, D. C., & Patterson, P. H. (2008). Intrabodies Binding the Proline-Rich Domains of Mutant Huntingtin Increase Its Turnover and Reduce Neurotoxicity. *Journal of Neuroscience*, *28*(36), 9013–9020. https://doi.org/10.1523/JNEUROSCI.2747-08.2008

Takegoshi, K., Nakamura, S., & Terao, T. (2001). 13C-1H dipolar-assisted rotational resonance in magic-angle spinning NMR. *Chem Phys Lett*, *344*(5–6), 631–637. https://doi.org/10.1016/S0009-2614(01)00791-6

Tao, A. J., Gadbois, G. E., Buczynski, S. A., & Ferguson, F. M. (2022). Targeted protein degradation: Emerging concepts and protein state-specific targeting principles. *Current Opinion in Chemical Biology*, *67*, 102114. https://doi.org/10.1016/j.cbpa.2021.102114

Thirumalai, D., Reddy, G., & Straub, J. E. (2012). Role of Water in Protein Aggregation and Amyloid Polymorphism. *Accounts of Chemical Research*, *45*(1), 83–92. https://doi.org/10.1021/ar2000869

Tuttle, M. D., Comellas, G., Nieuwkoop, A. J., Covell, D. J., Berthold, D. A., Kloepper, K. D., Courtney, J. M., Kim, J. K., Barclay, A. M., Kendall, A., Wan, W., Stubbs, G., Schwieters, C. D., Lee, V. M.-Y., George, J. M., & Rienstra, C. M. (2016). Solid-state NMR structure of a pathogenic fibril of full-length human α-synuclein. *Nat Struct Mol Biol*, *23*(5), 409–415. https://doi.org/10.1038/nsmb.3194

Ulamec, S. M., Brockwell, D. J., & Radford, S. E. (2020). Looking Beyond the Core: The Role of Flanking Regions in the Aggregation of Amyloidogenic Peptides and Proteins. *Frontiers in Neuroscience*, *14*, 611285. https://doi.org/10.3389/fnins.2020.611285

van der Wel, P. C. A. (2017a). Insights into protein misfolding and aggregation enabled by solid-state NMR spectroscopy. *Solid State Nucl Magn Reson*, *88*, 1–14. https://doi.org/10.1016/j.ssnmr.2017.10.001

van der Wel, P. C. A. (2017b). Insights into protein misfolding and aggregation enabled by solid-state NMR spectroscopy. *Solid State Nuclear Magnetic Resonance*, *88*, 1–14. https://doi.org/10.1016/j.ssnmr.2017.10.001

van der Wel, P. C. A. (2018). New applications of solid-state NMR in structural biology. *Emerging Topics in Life Sciences*, *2*(1), 57–67. https://doi.org/10.1042/ETLS20170088

Vasa, S. K., Singh, H., Grohe, K., & Linser, R. (2019). Assessment of a Large Enzyme–Drug Complex by Proton-Detected Solid-State NMR Spectroscopy without Deuteration. *Angewandte Chemie International Edition*, *58*(17), 5758–5762. https://doi.org/10.1002/anie.201811714

Wagner, A. S., Politi, A. Z., Ast, A., Bravo-Rodriguez, K., Baum, K., Buntru, A., Strempel, N. U., Brusendorf, L., Hänig, C., Boeddrich, A., Plassmann, S., Klockmeier, K., Ramirez-Anguita, J. M., Sanchez-Garcia, E., Wolf, J., & Wanker, E. E. (2018). Self-assembly of mutant huntingtin exon-1 fragments into large complex fibrillar structures involves nucleated branching. *J Mol Biol*, *430*(12), 1725–1744. https://doi.org/10.1016/j.jmb.2018.03.017

Walsh, T. R., & Knecht, M. R. (2017). Biointerface Structural Effects on the Properties and Applications of Bioinspired Peptide-Based Nanomaterials. *Chem Rev*, acs.chemrev.7b00139. https://doi.org/10.1021/acs.chemrev.7b00139

Wang, T., Jo, H., DeGrado, W. F., & Hong, M. (2017). Water Distribution, Dynamics, and Interactions with Alzheimer's β-Amyloid Fibrils Investigated by Solid-State NMR. *Journal of the American Chemical Society*, *139*(17), 6242–6252. https://doi.org/10.1021/jacs.7b02089

Wentink, A. S., Nillegoda, N. B., Feufel, J., Ubartaitė, G., Schneider, C. P., De Los Rios, P., Hennig, J., Barducci, A., & Bukau, B. (2020). Molecular dissection of amyloid disaggregation by human HSP70. *Nature*, *587*(7834), 483–488. https://doi.org/10.1038/s41586-020-2904-6

Zhao, X., Eden, M., & Levitt, M. H. (2001). Recoupling of heteronuclear dipolar interactions in solid-state NMR using symmetry-based pulse sequences. *Chem Phys Lett*, *342*, 353–361.